行政院國家科學委員會專題研究計畫　期中進度報告

子計畫一：釔鋇銅氧氧化物薄膜物理與元件研究(2/3)

計畫類別：整合型計畫
計畫編號：NSC93-2112-M-009-013-
執行期間：93年08月01日至94年07月31日
執行單位：國立交通大學電子物理學系(所)

計畫主持人：郭義雄
共同主持人：溫增明，莊振益，林俊源，吳光雄
計畫參與人員：鄭慧愷,賴良星,林東漢

報告類型：精簡報告
報告附件：出席國際會議研究心得報告及發表論文
處理方式：本計畫可公開查詢

中　華　民　國 94年5月31日

本年度研究成果可分為四部份:

(一).發現雷射濺鍍 perovskite 薄膜之成長機制。(在附錄一)

(二).於薄膜濺鍍成長過程，利用溫度緩慢增加，造成 adatom 加速擴散，量取 RHEED 隨溫度變化時之強度，利用強度在某特定最高值與 Kissenger 之固態反應理論模式，可逕取在薄膜初期成長時之附加原子之有效熱活化能。(在附錄二)

(三).利用微波量測研究高溫超導體之傳輸物理性質。

(四).微波元件研製。

釔鋇銅氧氧化物薄膜物理與元件研究進度報告

一、摘要

本計劃為利用微波量測研究高溫超導體之傳輸物理及其元件之特性。在本學年度內，我們不僅完成摻鈣的釔系薄膜($Y_{0.7}Ca_{0.3}Ba_2Cu_3O_{7-\delta}$)環形共振器及微帶線共振器的製備，並且藉由控氧技術，我們控制電洞濃度 p 從過摻雜至低摻雜區，致使我們可以在相同樣品上完成微波量測工作(包含不同頻率)。經由實驗和理論搭配間接得到複數電導率 $\sigma=\sigma_1-i\sigma_2$，發覺到實部 σ_1 跟虛部 σ_2 都具有一熱活化能隙(thermal activation gap)的存在，我們認為這個結果指出古典熱擾動(thermal fluctuations)在高溫態的超導物理行為上扮演一個很重要的角色。若與 Emery 和 Kivelson 的理論預言相較，頗具一致性的。再者，我們認為在薄膜樣品中，當 $T<T_c$ 時有約 300~400nm 之超導晶粒(superconducting grains)埋在非超導矩陣(non-superconducting matrix)中，這在強關聯電子系統常發現到，或許因為有長距離庫倫力與顆粒邊界所引起的效應，而這種不均勻結構可視為一種具雜亂性組合之 Josephson 接面網路，可以利用 percolation 理論與 X-Y 模型，用以分析 σ_1 和 σ_2 的特性。這個結果指出當降低溫度時這些超導對的電子流(或正常電流)會從一種激動 metastable state 到一種 stable state。以上這些結果指出 inhomogeneity 在此強關聯電子之超導傳輸動力行為中

扮演一個相當重要的角色。由此，提供在熱平衡時一些在不同電洞濃度 p 時一些有關物質性質的能量尺度，諸如熱擾動成對時之溫度、在長距有序參數形成之溫度等，幫助我們了解相分離(phase separation)現象與相熱擾動在不同材料參數條件下，巨觀的高溫超導傳輸物理性質。

二、計劃執行進度與結果

(一) 高溫超導物理

我們已經完成利用脈衝雷射蒸鍍法(PLD)在鋁酸鑭(LAO)基板上、下兩面蒸鍍摻鈣的釔系薄膜($Y_{0.7}Ca_{0.3}Ba_2Cu_3O_{7-\delta}$)跟釔鋇銅氧($YBa_2Cu_3O_{7-\delta}$) 薄膜等樣品的製作，藉由控氧技術，我們可以控制樣品氧含量的多寡，相當於控制樣品的電洞濃度，表一列出實驗的結果，我們採取以下的經驗公式來決定電洞濃度 p:

$$\frac{T_c}{T_{c,\max}} = 1 - 82.6(p - 0.16)^2, \qquad (1)$$

其中，T_c 為臨界溫度。對釔鋇銅氧($YBa_2Cu_3O_{7-\delta}$)薄膜而言，我們採取 $T_{c,\max} = 91K$ ，對摻鈣的釔系薄膜($Y_{0.7}Ca_{0.3}Ba_2Cu_3O_{7-\delta}$)而言，我們採取 $T_{c,\max} = 84K$ 。

Material	Oxygen content (7-?)	T_c (K)	Hole concentrations p
YBCO	6.95	91	0.160
YBCO	6.9	90	0.148
YBCO	6.85	86	0.134
YBCO	6.7	63	0.098
YBCO	6.6	54.5	0.090
YBCO	6.5	36.4	0.074
Ca-YBCO	6.95	60	0.218
Ca-YBCO	6.88	68.5	0.207
Ca-YBCO	6.85	78.5	0.188
Ca-YBCO	6.76	73.5	0.121
Ca-YBCO	6.74	68	0.111
Ca-YBCO	6.5	48.5	0.088

表一. 實驗結果與對應到各種不同的電洞濃度 p。

圖一顯示量測到釔鋇銅氧($YBa_2Cu_3O_{7-\delta}$) 薄膜隨不同電洞濃度變化其表面電阻 R_s 隨溫度變化的關係，從圖中很明顯的可以觀察到在溫度 T 接近臨界溫度 T_c 時，R_s 隨溫度變化的關係是先凹下再急劇的上升，很明顯具有一凹槽的特性，這種行為可用 critical slowing down 來說明， 圖二為該釔鋇銅氧($YBa_2Cu_3O_{7-\delta}$) 薄膜其表面電抗 X_s 在不同電洞濃度時隨溫度變化的關係，圖三顯示量測到摻鈣的釔系薄膜($Y_{0.7}Ca_{0.3}Ba_2Cu_3O_{7-\delta}$)隨不同電洞濃度變化其表面電阻 R_s 隨溫度變化的關係，在圖中我們觀察到 R_s 隨溫度變化的關係是一直在緩慢的上升，並不具有一凹槽的特性，相較於圖一釔鋇銅氧($YBa_2Cu_3O_{7-\delta}$)薄膜的結果有所不同，圖四為該摻鈣的釔系薄膜($Y_{0.7}Ca_{0.3}Ba_2Cu_3O_{7-\delta}$)其表面電抗 X_s 在不同電洞濃度時隨溫度變化的關係。接著，我們考慮一平面電磁波在

薄膜的表面上傳遞時，在 local electrodynamics 的限制下(mean free path l< penetration depth λ)，其表面電抗 Z_s = R_s + iX_s和複數電導率$\sigma = \sigma_1 - i\sigma_2$具有以下的關係:

$$Z_s = R_s + iX_s = (\frac{i\omega\mu_0}{\sigma_1 - i\sigma_2})^{1/2}. \quad (2)$$

(2)式經過換算後，我們得到實部電導率σ_1跟虛部電導率σ_2對 R_s和 X_s的等式，如下:

$$\sigma_1(T)=2\mu_0\omega XsRs/[Xs^2+Rs^2]^2, \quad (3)$$

$$\sigma_2(T)=\mu_0\omega[Xs^2-Rs^2]/[Xs^2+Rs^2]^2 . \quad (4)$$

圖五及圖六顯示釔鋇銅氧($YBa_2Cu_3O_{7-\delta}$)薄膜及摻鈣的釔系薄膜($Y_{0.7}Ca_{0.3}Ba_2Cu_3O_{7-\delta}$)隨不同電洞濃度變化其實部電導率$\sigma_1$隨溫度變化的關係，在將實部電導率$\sigma_1$對 5K 時的實部電導率$\sigma_1(5K)$歸依化之後對$T_c/T$做圖，結果如圖七所示，在$T/T_c < 0.1$，$\sigma_1/\sigma_1(5K) \approx 1$並且此結果和微觀結構的 disorder 無關，在$0.5T_c < T < T_c$時，由於熱擾動(thermal fluctuations)造成$\sigma_1/\sigma_1(5K)$急劇的下降。為了進一步分析這些實驗結果，我們採用這個公式$\sigma_1 = \sigma_1(5K)(1 - Ae^{-x \cdot T_c/T})$來擬合這些實驗結果，使用的軟體是"OriginR 7.0 SR0"程式，其中A和x是兩個擬合參數，擬合的結果在圖七中的實線跟表二。

Material	Oxygen content (7-?)	T_c (K)	λ(5K) nm	x	A	$E_{g0}(K)$	T^*(K)
YBCO	6.95	91	145			87.3±0.9	99.2±1.7
YBCO	6.9	90	150			86.4±0.9	98.2±1.7
YBCO	6.85	86	160			82.5±0.8	93.7±1.6
YBCO	6.7	63	170			60.4±0.6	68.6±1.1
YBCO	6.6	54.5	190			52.3±0.5	59.4±1.0
YBCO	6.5	36.4	265	0.96±0.01	2.41±0.03	34.9±0.3	39.6±0.6
Ca-YBCO	6.95	60	210			57.6±0.6	65.4±1.1
Ca-YBCO	6.88	68.5	165			65.7±0.6	74.6±1.2
Ca-YBCO	6.85	78.5	155			75.3±0.7	85.6±1.4
Ca-YBCO	6.76	73.5	170			70.5±0.7	80.1±1.3
Ca-YBCO	6.74	68	200			65.2±0.6	74.1±1.2
Ca-YBCO	6.5	48.5	250			46.5±0.4	52.8±0.8

表二.擬合實部電導率σ_1的擬合結果。

若我們定義$x \cdot T_c$(或$x \cdot k_B T_c$, 單位: meV)是一熱活化能隙(thermal activation gap, $E_{g1}(0)$),則當實部電導率σ_1為零時,我們得到另外一個特徵溫度$T^*_{\sigma 1} = \frac{x \cdot T_c}{\ln A}$,圖八顯示$E_{g1}(0)$ $T^*_{\sigma 1}$跟T_c對不同電洞濃度的變化圖,值得注意的是$T^*_{\sigma 1}$對p的變化,在低摻雜區時,接近 Emery and Kivelson 理論所預測的相位有序溫度上限(T_θ^{max}),在過摻雜區時,則接近平均場的溫度(T_{mean})。實際上,上面的擬合公式可以簡化為$\sigma_1(5K)(1 - e^{-E_{g1}(T)/k_B T})$,其中$E_{g1}(T) = E_{g1}(0) - E_{g1}(0) \times \frac{T}{T^*_{\sigma 1}}$,而此項$e^{-E_{g1}(T)/k_B T}$可被解釋為由於熱擾動造成相位失去的比重,在低溫區時($T/T_c < 0.1$),這一項的貢獻幾乎可以忽略,實部電導率σ_1幾乎達到飽和,事實上,在 5K 時的電導率$\sigma_1(5K)$跟量子電導(quantum conductance: $\frac{e^2}{h}$)是可以連接在一起,只要將量子電導除以一個幾何長度,進一步地,考慮到樣品晶粒的大小(約 300nm~400nm)相當於 Lee 理論的侷限長度(localization length, $\xi_L \approx 202nm$),而大於 quasiparticle 的 mean

free path($l \approx 75nm$)，我們認為在我們樣品內的準粒子(quasiparticle)是處於侷限態，那麼實部電導率σ_1就無法解釋是由準粒子在電磁場內運動造成的損耗，在圖九中顯示實部電導率$\sigma_1(5K)$跟5K時的超流體密度$1/\lambda^2(5K)$對不同電洞濃度的變化圖，結果顯示$\sigma_1(5K)$正比於$1/\lambda^2(5K)$，這個結果無法用古典的Drude模式來解釋，相反的，在巨觀量子穿隧現象裏，理論預期超流體在經由穿隧效應時，本質上會把損耗的能量傳給環境(environment)，因此，我們認為本實驗的實部電導率$\sigma_1(5K)$主要是由這個效應造成的。事實上，橫跨我們的環形共振器寬0.5mm約有1250~1700個晶界(grain boundaries)，在整個薄膜環形共振器則約有65×10^6~120×10^6個晶粒，很自然地，我們可以把這些超導晶粒看似放在非超導的矩陣上，利用一percolation模型，因為這些超導電流經由穿隧效應而串聯起來，當超導區域大於percolation threshold concentration $p_c = \int_{\sigma_c}^{\sigma_{\max}} d\sigma f(\sigma)$時，$f(\sigma)$為這種電導的分佈，我們認為每一個晶粒的電阻(或電導)彼此之間都會被束縛住，而這些被束縛住的電阻(或電導σ)是非常廣泛的分布在整個薄膜表面上。具體而言，percolation theory認為這種被束縛住的電導σ可以寫成$\sigma = \sigma_0 e^{-\Lambda\eta}$，其中$\eta$是均勻分布在0跟1之間，值得注意的是如果是一種thermal hopping的行為(potential barrier, ΔE)，則電導σ正比於$e^{-\Delta E/k_BT}$，而此時的電導分佈$f(\sigma) = \dfrac{1}{\Lambda\sigma}$，$\Lambda$代表這種分佈的寬度，

例如我們計算此時的 percolation threshold concentration $p_c = \int_{\sigma_c}^{\sigma_0} d\sigma f(\sigma) = \frac{1}{\Lambda}\ln\frac{\sigma_0}{\sigma_c}$，亦即 $\sigma_c = \sigma_0 e^{-\Lambda p_c}$，當 $\Lambda = \frac{1}{p_c}$ 時 $\sigma_c = e^{-1}\sigma_0$。在此分佈的情形之下，假若我們直接將電導 σ 取平均，則

$$<\sigma> = \int_{\sigma(\eta)}^{\sigma_0} d\sigma f(\sigma)\cdot\sigma = \frac{1}{\Lambda}(\sigma_0 - \sigma_0 e^{-\Lambda\eta}). \tag{5}$$

進一步地，若是經由 thermal hopping 而造成 percolation，則(5)式直接可寫成:

$$<\sigma> = \frac{\sigma_0}{\Lambda}(1 - e^{-\Delta E/k_B T}). \tag{6}$$

事實上，實驗結果也間接證實了 percolation 理論所預測的行為。

現在，我們採用跟 σ_1 相同的分析方法來分析 σ_2，亦即 $\sigma_2 = \sigma_2(5K)(1 - Be^{-y\cdot T_c/T})$，擬合的結果在表三，而從分析 σ_2 中也可得到另一個 thermal activation gap（$E_{g2}(0)$），所以 σ_2 也可寫成 $\sigma_2(5K)(1 - e^{-E_{g2}(T)/k_B T})$，其中 $E_{g2}(T) = E_{g2}(0) - E_{g2}(0)\times\frac{T}{T_{\sigma 2}^*}$。圖十顯示出 $T_{\sigma 2}^*$, $E_{g2}(0)$ 和 T_c（包含從 σ_1 得到的 $E_{g1}(0)$ 跟 $T_{\sigma 1}^*$），結果顯示 $T_{\sigma 1}^*$ 跟 $T_{\sigma 2}^*$ 幾乎是一樣的，我們認為這就是 Emery and Kivelson 所預測的相位有序溫度上限（$T_\theta^{\max}$）。

Material	Oxygen content (7-?)	T_c (K)	λ(5K) nm	y	B	$E_{g2}(0)$	$T^*_{\sigma 2}$(K)
YBCO	6.95	91	145			116.4±0.9	98.3±1.2
YBCO	6.9	90	150			115.2±0.9	97.2±1.2
YBCO	6.85	86	160			110.0±0.8	92.9±1.2
YBCO	6.7	63	170			80.6±0.6	68.0±0.8
YBCO	6.6	54.5	190			69.7±0.5	58.8±0.7
YBCO	6.5	36.4	265	1.28±0.01	3.27±0.04	46.5±0.3	39.3±0.5
Ca-YBCO	6.95	60	210			76.8±0.6	64.8±0.8
Ca-YBCO	6.88	68.5	165			87.6±0.6	74.0±0.9
Ca-YBCO	6.85	78.5	155			100.4±0.7	84.8±1.0
Ca-YBCO	6.76	73.5	170			94.0±0.7	79.4±1.0
Ca-YBCO	6.74	68	200			87.0±0.6	73.4±0.9
Ca-YBCO	6.5	48.5	250			62.0±0.4	52.3±0.6

表三.擬合虛部電導率σ_2的擬合結果。

最後，我們要強調以上這些實驗結果和微觀的 disorder 無關，我們樣品晶粒的大小(約 300nm~400nm)相當於 Lee 理論的侷限長度(localization length, $\xi_L \approx 202nm$)，而大於 quasiparticle 的 mean free path($l \approx 75nm$)，這個結果造成 quasiparticle 都被 localized，圖十一顯示一些能量尺度Δ_0, $E_{g2}(0)$, $E_{g1}(0)$, γ_0, ΔW and $\hbar/\tau$(分別從實驗得到或從 Lee 的理論推算出來)對不同電洞濃度p時的變化圖，其中Δ_0是能隙，ΔW是兩個 localized state 之 energy level 差，γ_0是 impurity band 跟$1/\tau$是 scattering rate，圖十一結果顯示出$\gamma_0 + E_{g1}(0) \simeq E_{g2}(0)$，然而這個結果的物理內涵為何仍舊有待進一度的釐清。

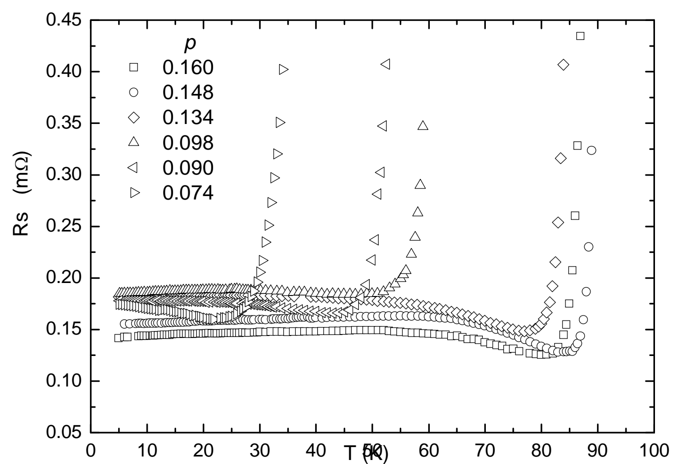

圖 1. 釔鋇銅氧薄膜隨不同電洞濃度變化其表面電阻 R_s 隨溫度變化的關係圖。

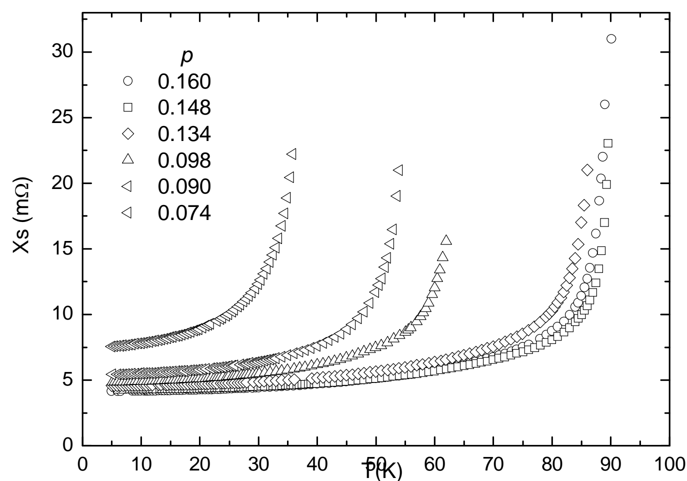

圖 2. 釔鋇銅氧薄膜隨不同電洞濃度變化其表面電抗 X_s隨溫度變化的關係圖。

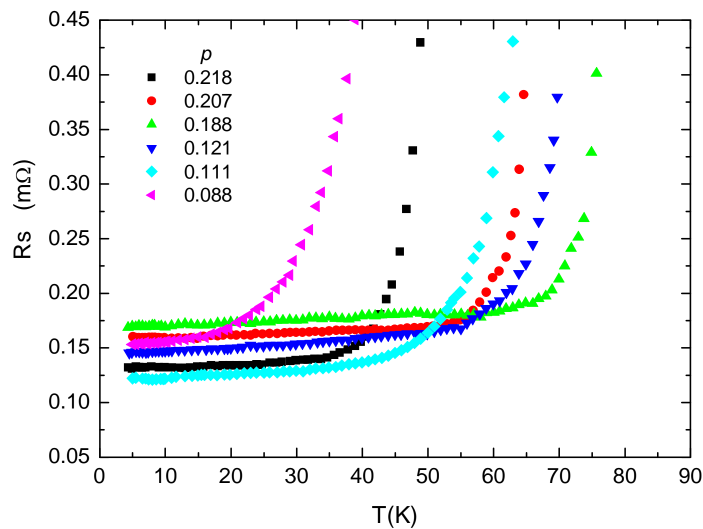

圖 3. 摻鈣的釔系薄膜($Y_{0.7}Ca_{0.3}Ba_2Cu_3O_{7-\delta}$)隨不同電洞濃度變化其

表面電阻 R_s 隨溫度變化的關係圖。

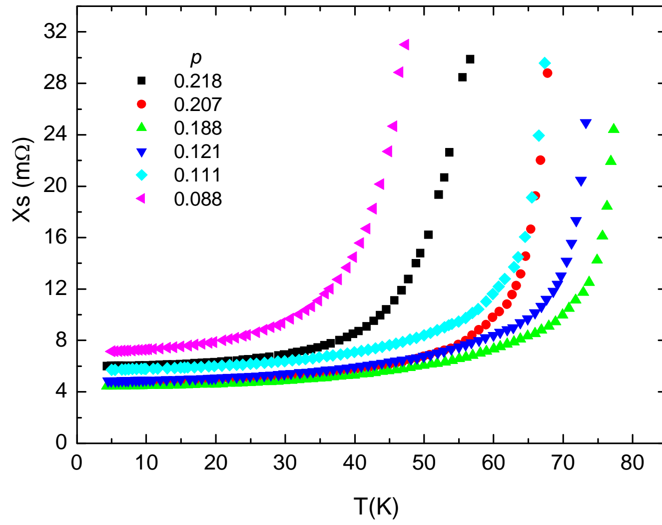

圖 4. 摻鈣的釔系薄膜($Y_{0.7}Ca_{0.3}Ba_2Cu_3O_{7-\delta}$)隨不同電洞濃度變化其表面電抗 X_s 隨溫度變化的關係圖。

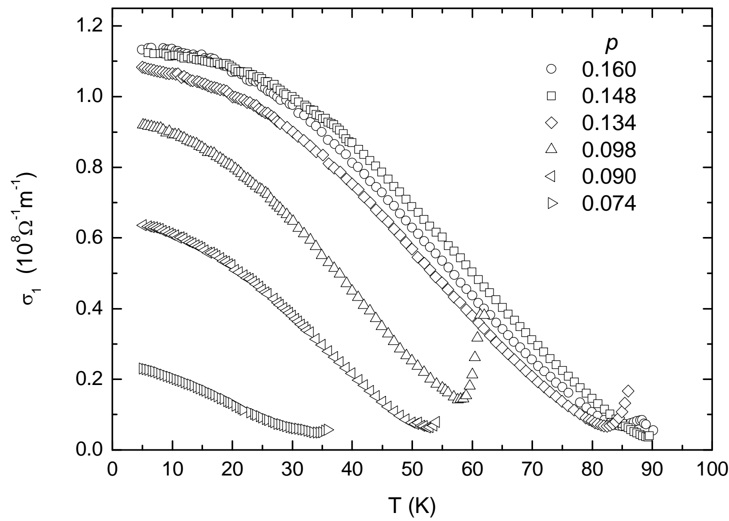

圖 5. 釔鋇銅氧薄膜隨不同電洞濃度變化其實部電導率σ_1隨溫度變化的關係圖。

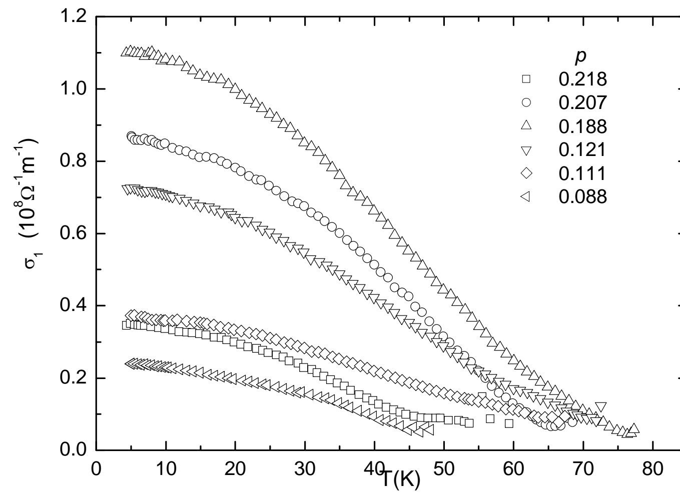

圖 6. 摻鈣的釔系薄膜($Y_{0.7}Ca_{0.3}Ba_2Cu_3O_{7-\delta}$)隨不同電洞濃度變化其實部電導率$\sigma_1$隨溫度變化的關係圖。

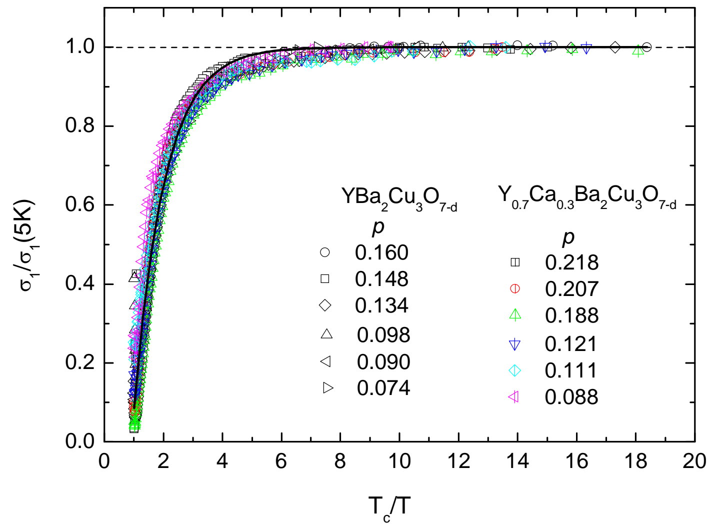

圖 7. 隨著不同電洞濃度變化$\sigma_1/\sigma_1(5K)$對 Tc/T 做圖，雖然電洞濃度不同，但幾乎都座落在相同曲線上，實線為數值擬合的結果。

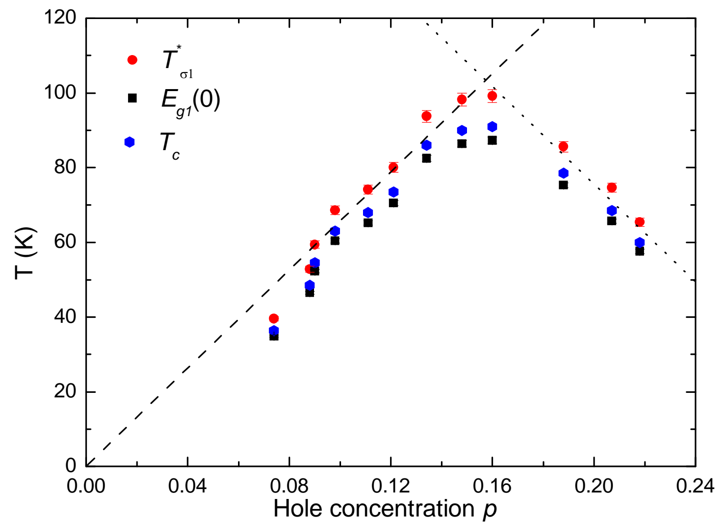

圖 8. 熱活化能隙$E_{g1}(0)$，$T^*_{\sigma 1}$跟 Tc 對不同電洞濃度的關係圖。

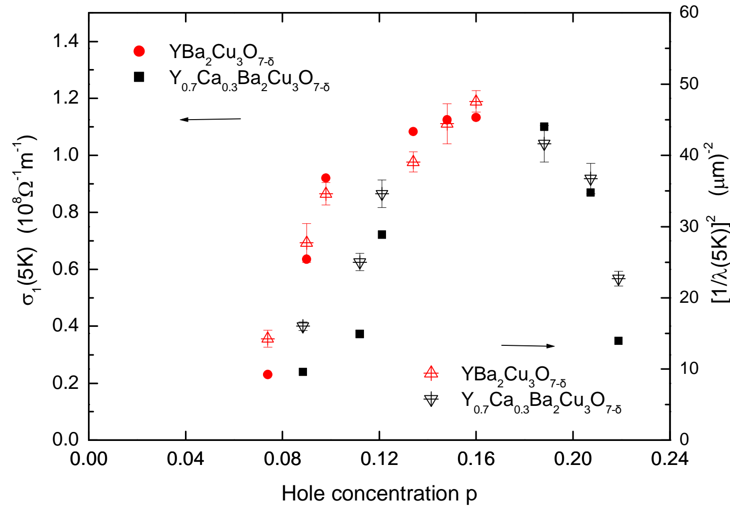

圖 9. 在 5K 時的實部電導率 $\sigma_1(5K)$ 跟超流體密度 $\frac{1}{\lambda^2(5K)}$ 分別對不同的電洞濃度作圖。

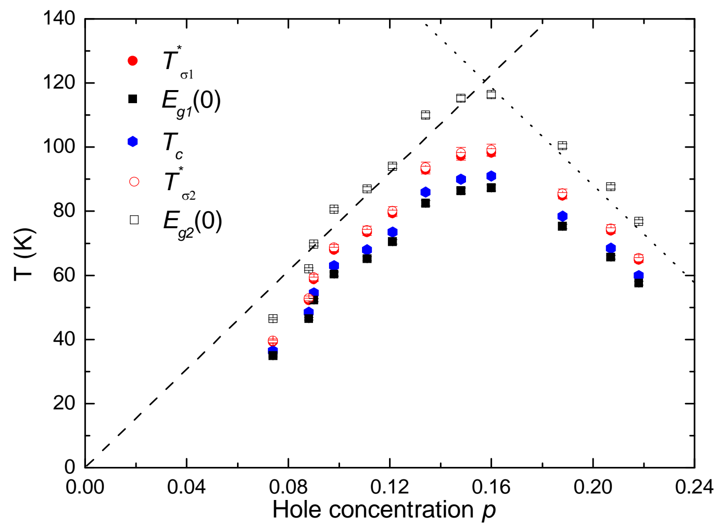

圖 10. 熱活化能隙$E_{g2}(0)$，$T^*_{\sigma 2}$，$E_{g1}(0)$，$T^*_{\sigma 1}$跟 Tc 對不同電洞濃度的關係圖，其中$T^*_{\sigma 2}$跟$T^*_{\sigma 1}$數值大小幾乎相同。

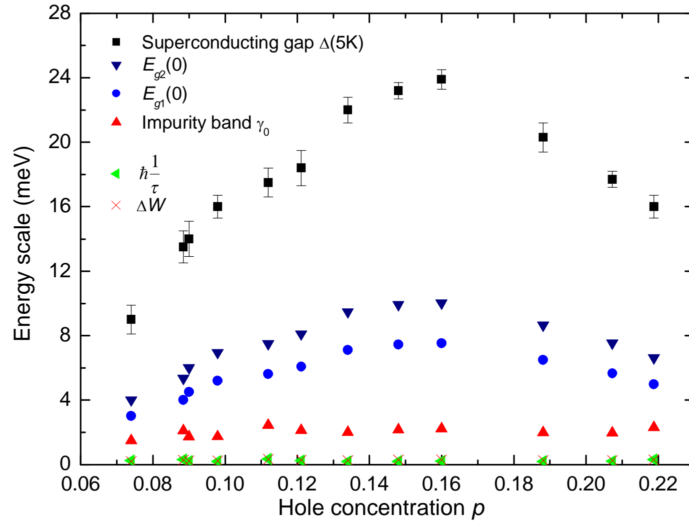

圖 11. 各種能量尺度Δ_0，$E_{g2}(0)$，$E_{g1}(0)$，γ_0，ΔW and $\hbar/\tau$ 對不同電洞濃度 p 時的變化圖。

（二）微波元件研製

一、微波元件

利用微小化的共振腔設計以及交錯耦合型結構的帶通濾波器（Fig.1）的架構，將中心頻率為 1.8GHz 的帶通濾波器製造在面積為 1×1 cm^2 的鋁酸鑭($LaAlO_3$)基板上，已達到濾波器尺寸微小化的目的，可降低成本。再配合零度與非零度饋入裝置，來設計高溫超導濾波器，其量測的結果（Fig.2）顯示，零度饋入式四階微型之交錯耦合型帶通濾波器的中心頻率在 1.816 GHz、比例頻寬為 3 %、通帶的插入損耗為 0.25 dB；非零度饋入式微型之交錯耦合型帶通濾波器的中心頻率在 1.811 GHz、比例頻寬為 2.8 %、通帶的插入損耗為 0.3 dB，此量測的結果與電腦模擬的結果大致吻合，零度饋入式的濾波器設計證明，在通帶插入損耗與截止帶的阻絕能力比非零度饋入式的濾波器佳。未來在應用上，不但能滿足通帶插入損耗小及高選擇性的需求，更能減少頻寬的浪費與雜訊的干擾。

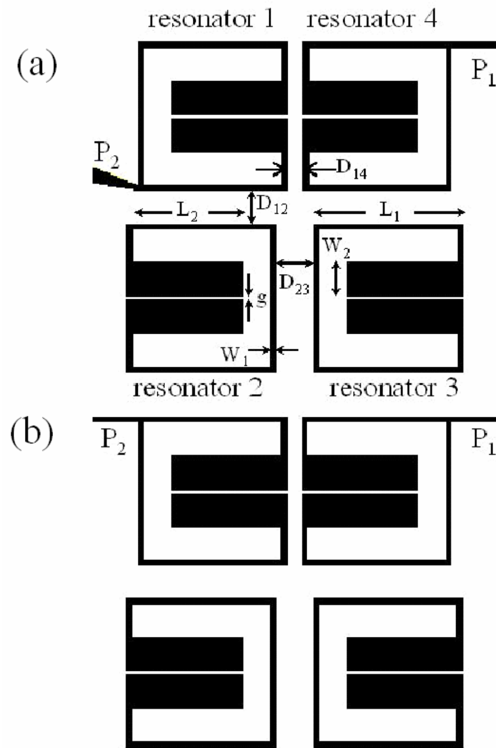

Fig. 1. Layout of the cross-coupled planar microwave filter with (a) symmetric (0° with P_1 and P_2) or (b) antisymmetric (180° with P_1 and P_2) feed structure used in this study. Geometric parameters for each resonator: W_1 = 0.1 mm, W_2 = 0.7 mm, L_1 = 3.1mm, L_2 = 2.3 mm, g = 0.1mm, D_{12} = 0.7 mm, D_{23} = 0.8 mm, D_{14} = 0.35 mm. respectively.

但美中不足的是，元件在製備上仍有以下兩項問題：

(1) 薄膜良率不穩定：

脈衝雷射蒸鍍系統，雖然有許多優點，但樣品的良率卻不穩定，即使在相同的鍍膜條件之下，鍍一大批樣品，每片薄膜的各項物理參數如表面平整度、薄膜平均厚度及臨界溫度值等，仍有些許差異。主要的因素來自於，基板的加熱溫度不均勻所致，因為基板與矽基板仍有空隙，導致基板加熱時，基板表面的溫度未能平均之下，以致於薄膜的磊晶成長不穩定。但任何一項物理參數未達標準，皆可

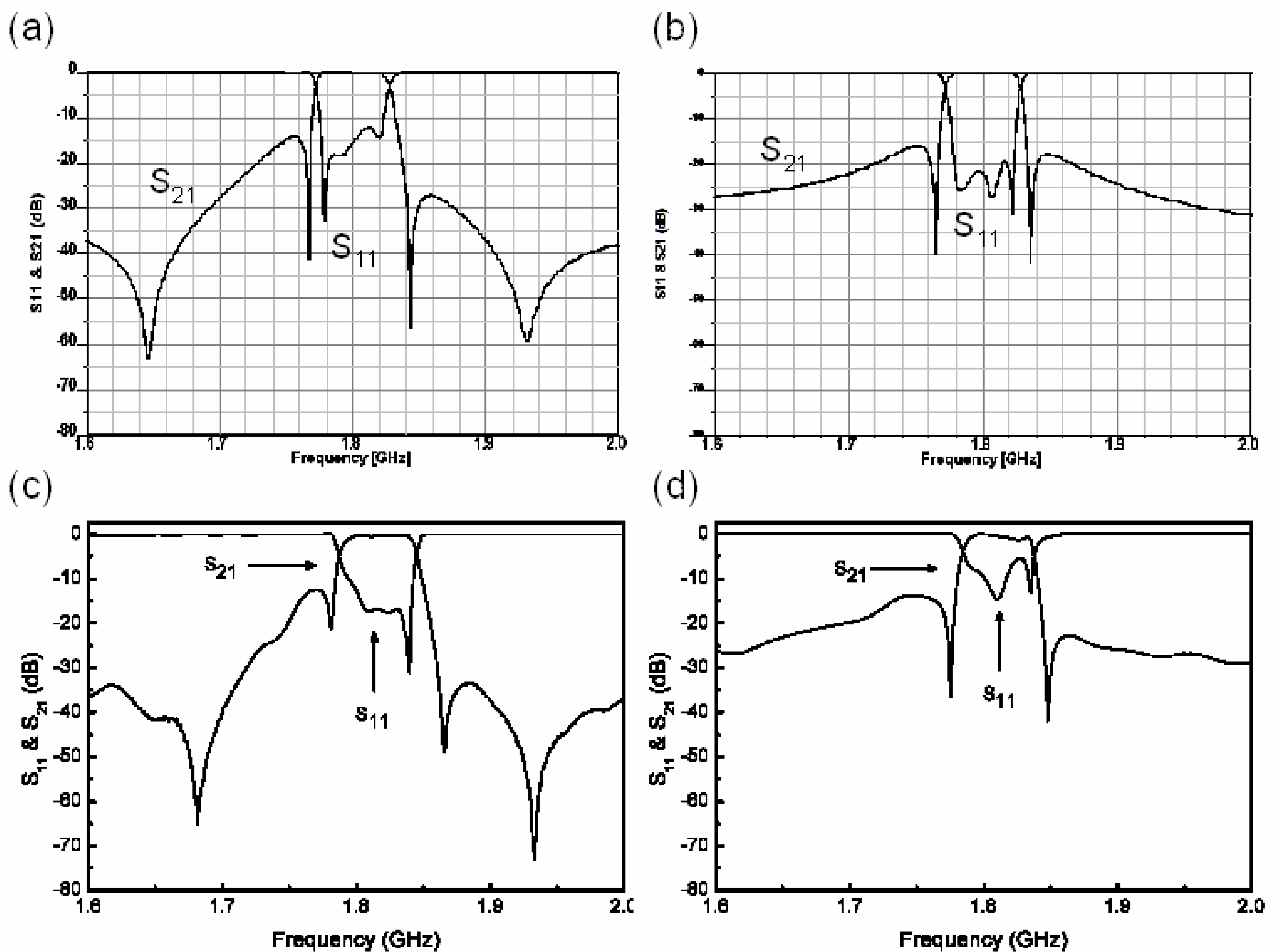

Fig. 2. The simulations of S21 and S11 responses for (a) symmetric and (b) antisymmetric feed structure filter and the measured results for (c) symmetric and (d) antisymmetric, respectively.

能導致濾波器元件的品質變差。

(2) 濕式微影蝕刻的問題：

本實驗是以濕式微影蝕刻的方式來製備高溫超導微波濾波器元件，用此方式蝕刻的線寬大約只能達數個 μm，而我們濾波器的最小線寬是 100μm，就我們的濾波器來講，微帶線邊緣的粗糙程度算是蠻大的。另外，濕式蝕刻的缺點，是還會造成線邊側蝕的現象，且依側蝕的程度不同，影響的程度亦不同，這些都會影響元件的效能表現。

二、未來展望

在製作高品質的濾波器，需要更穩定的製造方式，每個高溫超導薄膜的樣品，最好能維持在一定的水準，這樣在製備元件時，才不致於產生太大的誤差，因此提供兩種方法來減少實驗誤差：

(1) 改進薄膜良率穩定性：

採用基板背面黏銀膠的方式，以解決熱不均勻的問題，蒸鍍第一面薄膜的厚度要鍍很厚，當作接地面用，對於元件的效能影響不大。在蒸鍍第二面的時候，第一面薄膜直接上銀膠，而第一面薄膜夠厚在加熱時，銀膠也比較不容易貫穿第一面薄膜，因此解決了加熱不均勻的問題後，相對薄膜的表面平整度與厚度均勻也會改善，藉此以提升鍍膜的良率的穩定性。

(2) 改進蝕刻方式：

採用濕式蝕刻在先天上本來就有其限制，所以若是以此種方式來製作微波濾波器，在我們所要求的線寬下，邊緣參差不齊是無可避免的。所以若是以更好的乾式蝕刻技術來製作濾波器的話，例如：離子蝕刻(Ion Milling)或電子束微影蝕刻(E-Beam Lithography)技術，這樣邊緣輻射的效應勢必可以減少。

最後，未來我們希望能使讓濾波器的尺寸更微小化以降低成本。最直接的方法是，利用更密集化共振腔結構圖形的設計技術之外，或是使用介電常數較高的基板，例如 TiO_2 基板(ε_r=105)，可縮小濾波器中共振腔的長度，間接達到縮小整體元件的尺寸。利用以上兩個方法均可達到縮小濾波器尺寸的目的。

附錄一：

Dynamics of Film Growth of Perovskite-Type Materials by Laser Ablation from RHEED Observations

Y. S. Gou, J. Y. Lee, K. H. Wu and J. Y. Juang
Department of Electrophysics National Chiao Tung University, Hsinchu, Taiwan

Abstracts

Kinetic mechanism of thin film-growth using laser ablation from RHEED observations has been presented to examine the details of growing processes of STO thin films as temperature increasing smoothly. Using **Langevin-like force-balanced equation for dislocation movements** we can interpret the physical implications of the experimental observations. The model shows dislocation-mediated melting phenomena in two dimensions, and can be generalized to understand the growth mechanism of thin films of **Perovskite-Type materials** at their initial stage using laser ablation technique.

Introduction

RHEED intensity oscillations were first observed for GaAs(001) homoepitaxy grown by molecular beam epitaxy (MBE) and were interpreted as a manifestation of a two-dimensional (2D) layer-by-layer growth [1-2]. During the past decades, RHEED has become a powerful technique for monitoring the epitaxial growth of pulsed laser deposited (PLD) perovskite-oxide thin films [3].

For explaining the RHEED intensity oscillations during film growth related to its growth mechanism, we have present a model that step edges dominate the scattering of the electron beam [3]. The intimate correspondences between the RHEED intensity oscillations and the variations of step edge density in an evolving growth surface have already been successfully justified the above relations in the deposition of STO thin films using PLD technique [3, 4].

In this report, a continuous annealing scheme by increasing temperature instead of fixed temperature annealing was studied in order to investigate the initial-stage growth mechanism of homoepitaxial STO films. It is anticipated that the current study will provide an exact knowledge of the growth mechanism of perovskite thin films using laser ablation technique with various annealing schemes at somewhat proper temperature. Based on the characteristic features observed in the experiment, which show a great consistency with the prediction by the dislocation-mediated melting in two dimensions [5, 6], a model of growth kinetics related to the Brownian movements of the dislocation in the system will be proposed in terms of Langevin-like force-balanced equation. The physical implications of the essential effects relevant to the model construction will be discussed. Especially, the significance of the damping force, elastic force and thermal creep force of the dislocation in the system during growth will be indicated.

Experiment

The detailed experimental processes can be seen in our previous work [7]. In what follows only some important facts related to the model construction are mentioned. A KrF excimer laser with pulse duration of 30 ns, operated primarily at a repetition rate of 1 Hz, was used to deposit four samples under essentially the same conditions. The target was a single crystalline disk of STO. The films were deposited

at ambient temperature with an oxygen partial pressure of 5×10^{-4} Torr. Each film contains presumably the same amount of deposited material delivered by 500 laser pulses with which the growing film can maintain the state of low-supersaturation. The films were then subjected to *in-situ* continuous annealing at different heating rates by adjusting the current applied to the heating resistive block. The heating rate used in the present study ranges from 20℃/min to 35℃/min.

During the whole process, the intensity of the RHEED specular beam was closely monitored following the setups described in detail previously [7]. Briefly, a 20 keV electron beam was directed along the [100] direction of STO substrate with a grazing angle of 0.7°. With a de Broglie wavelength of about 0.86 Å, the grazing electron beam is slightly off-Bragg conditions and the RHEED intensity is expected to be most sensitive to the step edges on the surface [1].

Figure 1(a) shows the RHEED intensity as a function of the elapsed time for the four different continuous annealing schemes. Curves (1) to (3) are the results of RHEED intensity evolution obtained by heating the films with fixed temperature increasing rate. The heating rates were 35℃/min, 25℃/min, and 20℃/min, respectively. On the other hand, curve (4) obtained heating the film at 25℃/min before it reached 400℃. The sample was kept at 400℃ for about 60 seconds and then followed by a rate of 15℃/min toward the end of the process. As is evident from the results, all the four annealing schemes display qualitatively the same manner. The precipitous drop of RHEED intensity at the commencement of deposition is indicative of sudden increase in step-edges density on the growing surface [4]. While the retention of very low intensity (the diffraction spots almost faded out) without any noticeable oscillating behavior implies that there is essentially no island coalescence until certain threshold temperature. This is better visualized by re-scaling the time axis with temperature. As shown in Fig. 1(b), with such re-scaling, all the four curves exhibit essentially the same behavior.

In all cases, when temperature approaches 660℃, there are two distinct phases observed. Namely, the steep rise of RHEED intensity is manifested by sudden appearances of the diffraction spots and the phenomena seem to be independent of heating rate. Within the context of the step edge model [3], the current results suggest a drastic change in film surface morphology occurred at 660℃.

For the kinetic approach, the differential properties of RHEED intensity, dI/dT, are derived from the above curves, as shown in Fig. 2. It can be observed that the curves for dI/dT are unchanged before 660°C, then there is a resonance-like peak occurred, where the maximum is located at temperature, around 690°C. After 720°C, the behaviors of dI/dT are either rising steadily or maintaining constant.

Discussion

In the light of statistical physics scenario, we have to ask a question about what kind of active object plays a role of independent Brownian particle in the growing system. In fact we will take dislocation "as the object of the Brownian particle". The reasons are given as follows; First, nearly all crystals in nature grown at low supersaturation, which is mentioned previously as the state in our experiment, will contain dislocations, as otherwise they could not have grown [8]. Second, the experimental observations show closely the dislocation-mediated melting phenomenon in two dimensions [5, 6]. Therefore it may be better described the growing process as a system of

thermal-activated motion of dislocations as temperature increasing in our work. The model based on the dislocation of Brownian-movements, which is closely analogous to superconducting flux-creep in individual pinning problem [9], will be formulated. Based on the experimental observations and the model assumptions, we get the following physical scenario. On the one hand, when the temperature below 660 ^{o}C the state of the system is in the solid phase, which can also be described as the pinning static state of the dislocations. On the other hand, when the temperature higher than T_{KT}, which is defined as Kosterlitz-Thouless temperature, the solid is melting, Langevin-like force balance equation will be applied to get the dynamic evolution of the system in thermal equilibrium.

Here, we will depict the salient features of forces acted on the dislocation within crystal in a small island. First, the thermal creeping force, F(T), of the dislocation resulted from the increasing temperature is assumed to be analogous to the flux-creep theory in superconducting problems as suggested by Anderson and Kim [9]. Moreover, F(T) can be replaced by F(t) because of the constant temperature rising rate. Second, an elastic force, which is due to plastic deformation with the existence of the dislocation within the crystal, is assumed to obey the Hook's law. The density of the dislocations is so dilute that the pinning can be visualized as an individual one and each dislocation is assumed to be independent. In this situation, the elastic constant will be taken as constant and independent of temperature. And last, the viscousity force, βυ, is assumed in the irreversible process.

In the pinning static state, when $F(t) < F_p$, where F_p is the threshold pinning force of the dislocation pinning, the system is static. When $F(t) > F_p$, the thermal force exceeds the pinning force as $T > T_{KT}$, where T_{KT} is the K-T transition temperature from solid to fluid phase in two-dimensional problems [5]. Then the Langevin force-balanced equation can be utilized to describe the dynamic evolution of the dislocation in the latter case.

$$md^2r/dt^2 = -\beta\upsilon - k\, r + \gamma t - F_d \qquad (1)$$

where r is the ensemble average displacement of the dislocation, υ is the velocity, m is an effective mass of a dislocation, β is the damping coefficient, k is the elastic constant, γ is a constant and γt - F_d is described as the external force originated from the thermal creep effect of the dislocation and F_d is the temperature independent dynamic frictional force arising from the atomic roughness surface. Finally, the inertial term is arisen from the condition that temperature rising time is much faster than any characteristic times of the forces acted on the dislocation in the equation (1), which will be justified in our model below.

The dotted line shown in curve (1) of Fig. 3 is the preliminary fit to the experimental data using Eq. (1) with β=0.8, m=24, k=0.007, γ=0.3, F_d=460, and threshold pinning force of F_s=500. Note that the relaxation time due to the viscousity m/β is about 30 sec, and the elastic relaxation time is about 280 sec, the relaxation due to the creeping is about 80 sec. All these characteristic times are much larger than the dt (~3.0 sec) in equation (1). Except for small deviation with curve (1) due to the rounding before the onset of dislocation motion, the curve is in satisfactory agreement with the experimental curves shown in Fig. 3. Whatsoever, it is indicative that, in the dynamical regime of STO homoepitaxy, the damping and kinetic friction are playing prominent roles in determining the coalescence process of growing islands.

The physical picture of the growing processes in terms of the model can be given as follows.

When the annealing temperature T begins to increase from the room temperature, the thermal activated force to push the Brownian-like dislocation in the direction along the pressure gradient decreasing will become larger and larger and is possibly to pull the dislocation away from the initial fixed position with the thermal activation. Here the center-of-mass displacement "*r*" of the dislocation is assumed proportional to 1/L where L is the step edge length per unit area. As can be seen, if the step edge length becomes shorter due to the effect of island growth, the dislocation will move a corresponding longer distance. It means that the inverse of the length of step edge, 1/L, is analogous to the displacement of the dislocation. Therefore, the larger displacement of the dislocation will have the higher step-edge density and thus the higher probability of the attachment of the mobile adatom to island edge or/and vacancy in the front of growing surface to make the coalescence effect.

Moreover, there are some interesting behaviors of such Brownian motion are worthy discussing. The relations between the force acted on the Brownian-like dislocation and temperature are shown in Fig.4. In the figure, it shows that although the thermal-activation force and pinning force are much larger compared to the elastic force and damping force, but the small elastic and damping force dominate the microstructure in the system of thin film. It clearly predicts such small values of k and β to determine the thin film growth models. And the relations between the dislocation's acceleration and temperature are also shown in Fig 5. It shows that the larger elastic constant will cause the faster variation of deceleration. In Figs. 4 and 5, another feature is worthy nothing that the elastic and damping force are competed with each other during redistribution of surface coverage. At the melting stage, dislocations begin moving and the damping force is dominated, but elastic force gradually become important while the displacement of the Brownian-like dislocation is large enough toward the high temperature end. When the elastic force is equal to the damping force, we found that dI/dT reaches the maximum at T_R.

In summary, the kinetics of surface morphology evolution of pulsed laser deposited STO films were investigated by monitoring the RHEED intensity variations during the continuous temperature-increasing annealing scheme. An abrupt increase of the RHEED intensity was observed around 660℃, which corresponds to the K-T transition temperature in each annealing process. Moreover, within the context of step -edge model all the results were interpreted how to decrease surface step-edge density induced by Brownian-like dislocation dynamics in thermal equilibrium with various temperature ranges. By analogizing the temperature derivative of the RHEED intensity to the effective velocity of Brownian-like dislocation movements, the experimental results are satisfactorily described by a Langevin-type force-balanced equation, which stems from the idea of the flux-creep theory in the superconductivity. Finally, the present results provide a definite way of identifying an optimum temperature range for controlling the epitaxial growth kinetics and hence of the resultant epitaxial films for various Perovskite-Type materials using PLD technique.

ACKNOWLEDGEMENTS

Research supported by the National Science Council of Taiwan under grants NSC89-2112-M009-048 and NSC89-2112-M009-049.

REFERENCES

1. J. H. Neave, B. A. Joyce, P. J. Dobson, and N. Norton, Appl. Phys. A **31**, 1 (1983).
2. J. M. Van Hove, C. S. Lent, and P. I. Cohen, J. Vac. Sci. Technol. B **1**, 741 (1983).
3. J. Y. Lee, J. Y. Juang, K. H. Wu, T. M. Uen, and Y. S. Gou, Surf. Sci. **449**, L235 (2000).
4. T. C. Wang, J. Y. Juang, K. H. Wu, T. M. Uen, and Y. S. Gou, Japanese Journal of Applied Physics 43, 771 (2004).
5. D. R. Nelson and B. I. Halperin, Phys. Rev. B **21**, 5312 (1980).
6. J. M. Kosterlitz and D. J. Thouless, J. Phys. C6, 1181 (1973).
7. J. Y. Lee, Phd dissernation, Institute of Electrophysics, National Chiao-Tung University (2001).
8. C. Kittel, Introduction to Solid State Physics (John Wiley? Sons, Inc., Singapore, 1986).
9. P. W. Anderson, Phys. Rev. Lett. 9, 309 (1962); P. W. Anderson and Y. B. Kim, Rev. Mod. Phys. 36, 39 (1964).

Figure Captions

Figure 1: (a) The RHEED intensity as a function of time with heating rate of (1) 35℃/min (2) 25℃/min, (3) 20℃/min, and (4) 25℃/min for T<400℃ and 15℃/min for T>400℃. (b) Same as (a), except that the x-axis has been rescaled to temperature.

Figure 2: The temperature derivative of the RHEED intensity curves shown in Fig. 1(b). The dotted curve is the fit to the model discussed in the text.

Figure 3: By changing the k values of Eq. 1, the calculation of the model show the slightly different character after the peak. The temperature of the resonance-like of curve (3) is denoted as T_R.

Figure 4: The origin of the forces in the model, which uses the same parameters setting of curve (3) in figure 3. The temperature of the resonance-like is denoted as $T_{R.}$ (a) Thermal-activation force (b) Pinning force (c) Elastic force (d) Damping force.

Fig. 5: The model calculation which shows the relation between the dislocation's acceleration and temperature.

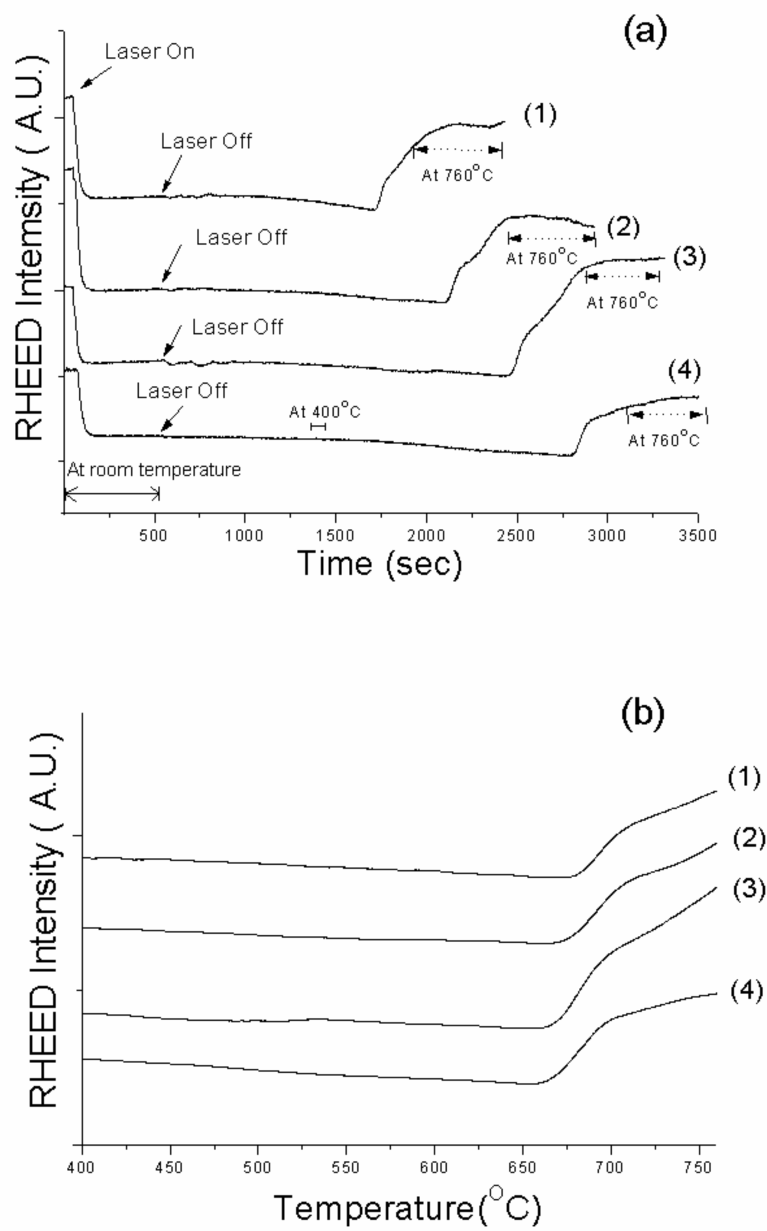

Fig. 1 of 5.

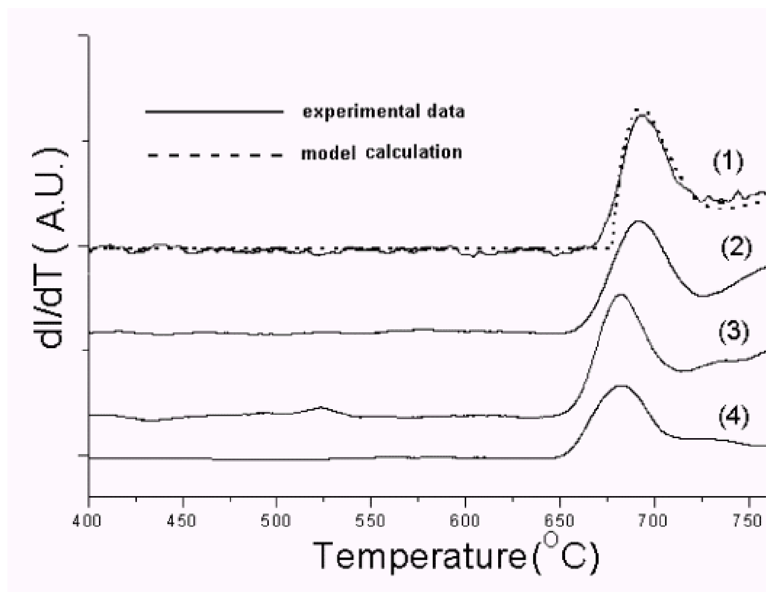

Fig. 2 of 5.

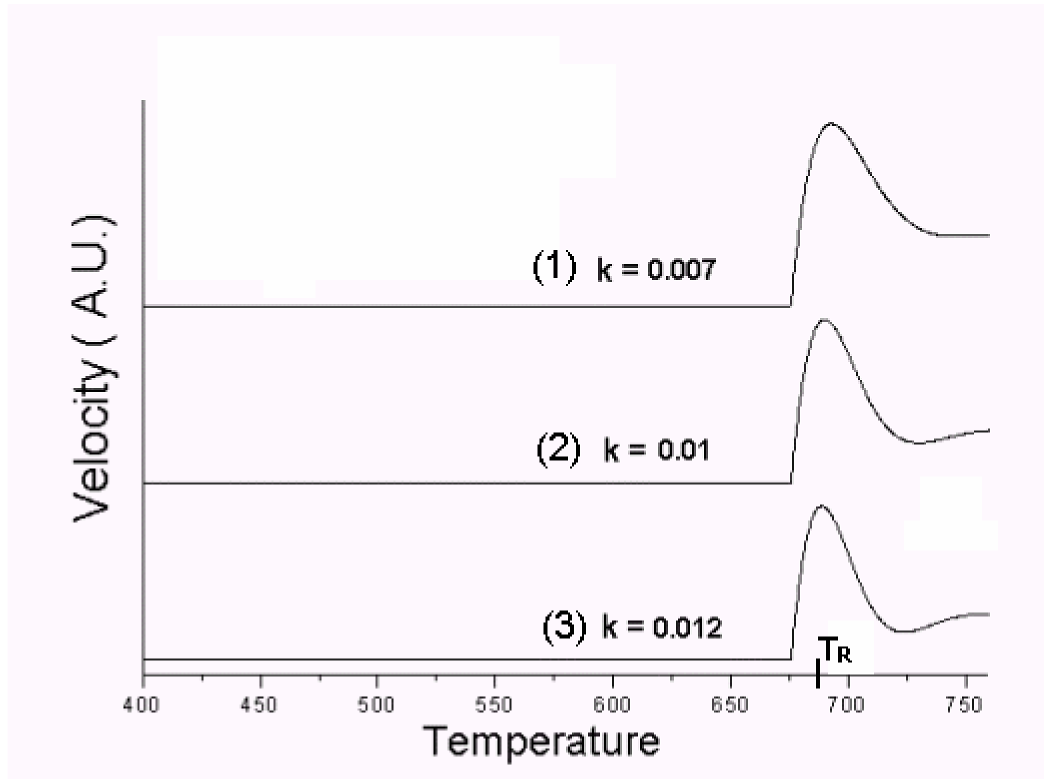

Fig. 3 of 5.

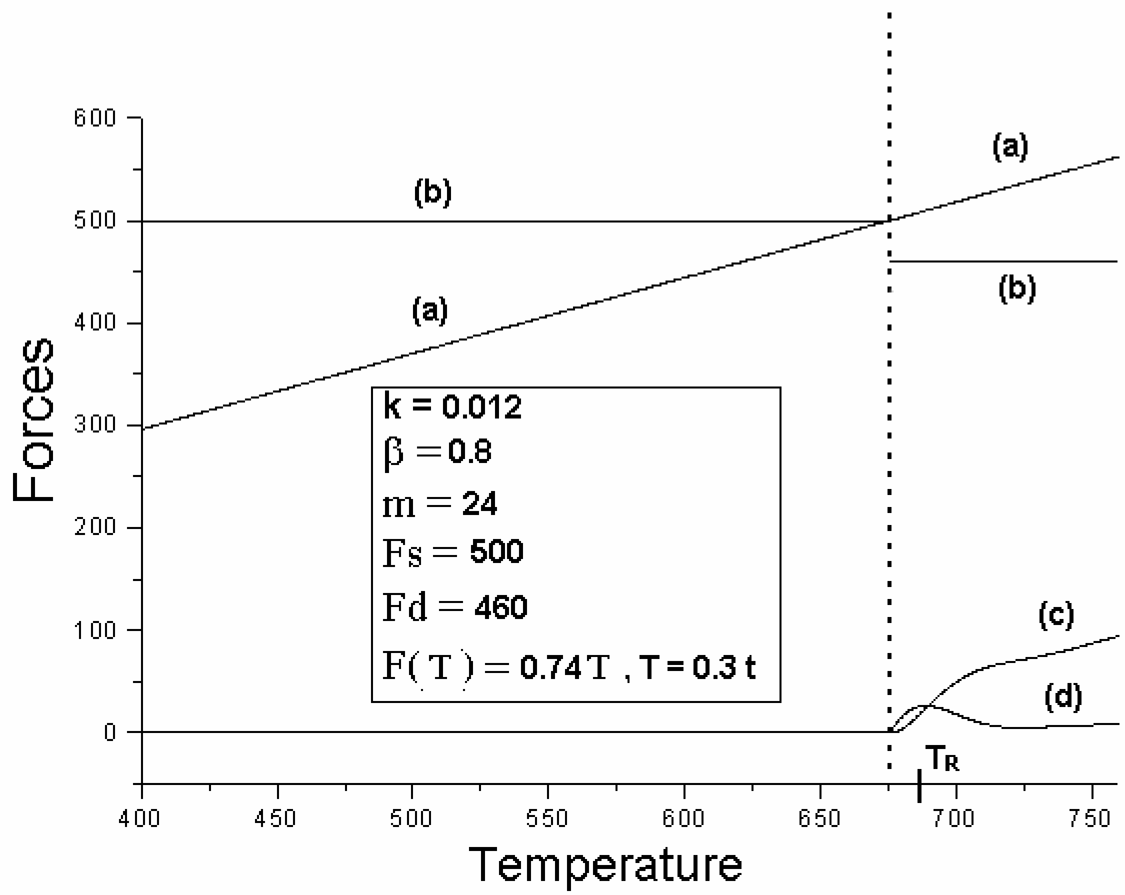

Fig. 4 of 5

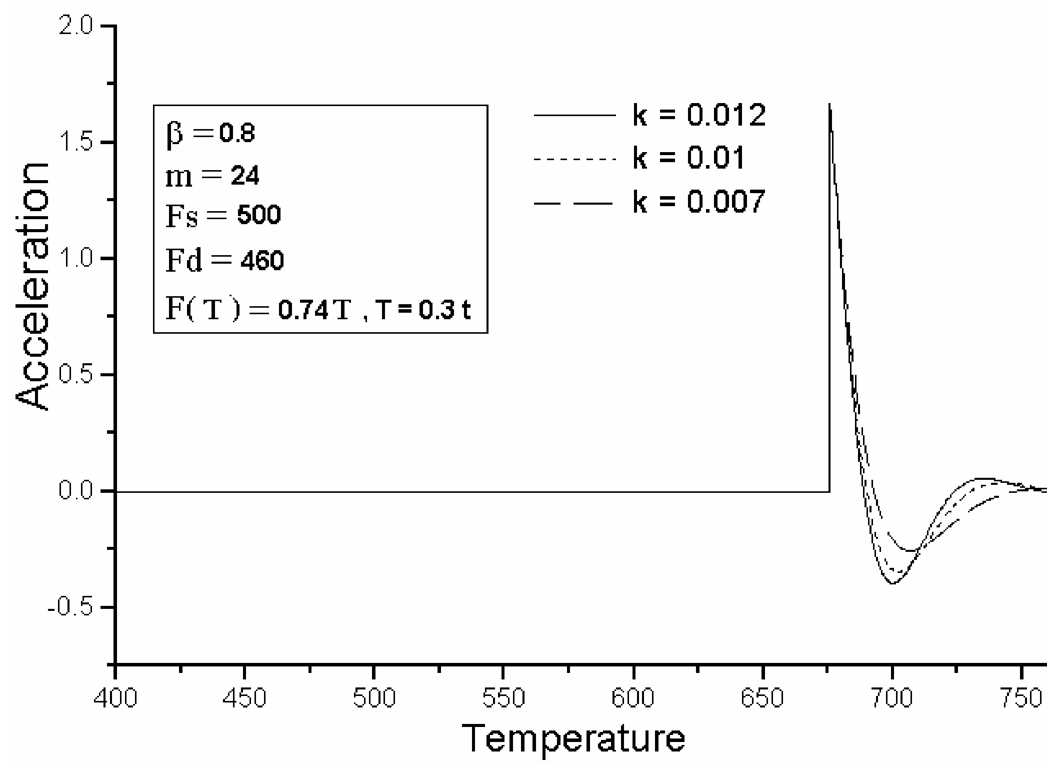

Fig. 5 of 5.

附錄二:

Japanese Journal of Applied Physics
Vol. 44, No. 2, 2005, pp. 1067–1068
©2005 The Japan Society of Applied Physics

Brief Communication

Activated Kinetics of Room-Temperature-Deposited $SrTiO_3$ Thin Films Investigated by Reflection-High-Energy-Electron-Diffraction-Monitored Annealing at Different Heating Rates

Te-Chun WANG, Jung-Yuee LEE, Chih-Chang HSIEH, Jenh-Yih JUANG, Kaung-Hsiung WU, Tzeng-Ming UEN and Yih-Shun GOU

Department of Electrophysics, National Chiao-Tung University, Hsinchu 300, Taiwan

(Received July 1, 2004; accepted October 25, 2004; published February 8, 2005)

A series of reflection-high-energy-electron-diffraction-monitored annealings with different heating rates have been conducted on Strontium Titanate films deposited by laser ablation at room temperature. All the films exhibited a steep RHEED intensity rise above 660°C during annealing with increasing temperature. The peak temperatures of the intensity derivatives were found to shift at different heating rates, suggesting an activated surface state transition. A Kissinger type plot of the peak temperatures showed an effective activation energy of 4 eV. [DOI: 10.1143/JJAP.44.1067]

KEYWORDS: RHEED, activation energy, reflection high-energy electron diffraction, Kissinger plot, kinetics

The oscillation of reflection high-energy electron diffraction (RHEED) intensity has long been used to monitor the layer by layer growth during molecular beam epitaxy.[1] The oscillating intensity quantifies the extent of completion of a nucleation-growth-coalescence growth cycle. The RHEED oscillation can also be regarded as a rate competition between the adsorption of source materials and the diffusion of adatoms. The reflected electron intensity increases as the rate of deposition and cluster nucleation is smaller than that of the island growth and diffusion. It is therefore of great importance to obtain quantitative information on the kinetics of the surface diffusion and the nucleation for understanding correlation between the layer-by-layer growth mechanism and the RHEED intensity oscillation.

The RHEED specular electron beam intensity was found intimately related to the surface edge defects of epitaxial films.[2,3] The activated kinetics of the defect evolution and surface diffusion particularly the activation energy calculation can be made from the RHEED intensity.[4,5] In ref. 4, comparisons of RHEED oscillation curves of fixed deposition temperatures were made to decide a series of transition temperatures from the layer-by-layer growth mode to the step flow mode. The Arrhenius plot was then made with the transition temperature and the diffusion lengths defined by a series of deposition rates. In ref. 5 the RHEED-monitored anneal recovery of interrupted deposition was used to deduce an exponential characteristic time for the diffusion Arrhenius plot. Besides these two methods, we conducted a series of RHEED-monitored constant temperature annealing of strontium titanate epitaxial films to investigate the diffusion kinetics.[3,6] By considering the connection between the film surface edge defect density and the RHEED intensity, we found a quadratic power law dependence of the RHEED intensity with respect to anneal time. A diffusive activation energy of the order of 1 eV was obtained from the Arrhenius plot.[7]

The interrupted deposition experiment of constant temperature annealing provided good epitaxial films. On the other hand, low-temperature deposition might reveal other useful information for films with an extremely high defect density or near the amorphous state. A series of room temperature deposition of strontium titanate were conducted.[8] A KrF excimer laser with a pulse duration of 30 ns and 1 Hz repetition rate was used to deposit four samples under similar conditions. The target was a single-crystal disk of STO 15 cm away from the deposited substrate. The deposition energy density was $2\,J/cm^2$. All films were grown onto as-polished STO(100) substrates attached to a resistive heating stage. The films were deposited at ambient temperature with an oxygen partial pressure of 5×10^{-4} Torr. Each film contains the same amount of source material delivered by 500 laser pulses. The films were then subjected to *in-situ* continuous annealing at different heating rates. A 20 KeV electron beam was directed along the [100] direction of the STO substrate with a grazing angle of 0.7°. With a de Broglie wavelength of approximately 0.86 Å and a lattice constant of 3.79 Å, the grazing electron beam is under slightly off-Bragg conditions and the RHEED intensity is expected to be more sensitive to the step edges on the surface.[1]

The RHEED intensities of four different heating rates are shown in Fig. 1. Curves (1) to (3) show the results for fixed heating rates of 35°C/min, 25°C/min and 20°/min respectively. Curve (4) was obtained by heating the film at 25°C/min before reaching 400°C and maintaining the temperature constant for 1 min and finally heating at a rate of 15°C/min to 760°C. The sudden drop in RHEED intensity, accompanying the disappearance of RHEED spots, of all curves when the laser was turned on represents the introduction of a large amount of beam-diffracting defects. During the room-

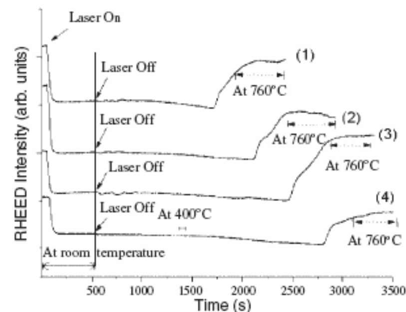

Fig. 1. RHEED intensity as function of time at heating rates of (1) 35°C/min, (2) 25°C/min, (3) 20°C/min (4) 25°C/min for $T < 400$°C and 15°C/min for $T > 400$°C.

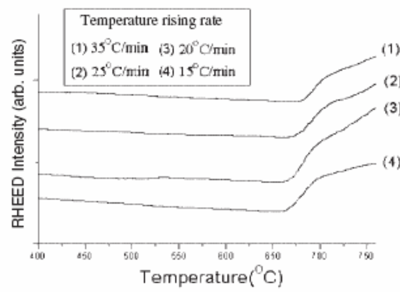

Fig. 2. Same as Fig. 1 except that the *x*-axis has been rescaled to temperature.

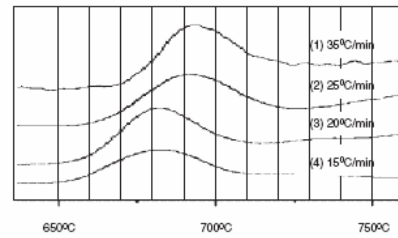

Fig. 3. Enlarged peak region of the temperature derivative of the RHEED intensity curves shown in Fig. 2. The peak temperatures are estimated as 693, 691, 682 and 681°C for heating rates of 35°C/min, 25°C/min, 20°C/min and 15°C/min, respectively.

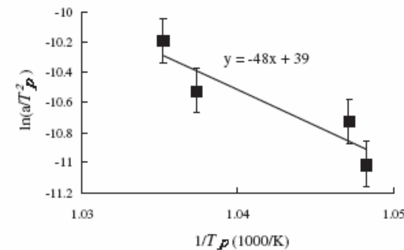

Fig. 4. Kissinger plot with RHEED intensity derivative peak shift. An effective activation energy of 4 eV is obtained.

temperature deposition no sign of RHEED intensity increase can be detected, implying the diffusion mechanism is excluded at low temperature. *Ex situ* surface examinations including reflective X-ray analysis were conducted on our room temperature deposited STO films.[9] The results indicated that the films were composed of a poorly crystallized flat layer. From the X-ray reflectivity fitting method as detailed in ref. 9 and the cited references therein, the density of the deposited material is estimated at 90% that of a perfect crystal. Therefore it can be considered a poorly crystallized solid with almost no reflection for grazing electron beams. All intensity curves experienced a similar steep rise at the end period of the heating treatment. Converting the time scale to the corresponding temperature scale (Fig. 2), we noticed that all the intensity curves start to rise at the temperature region slightly above 650°C and extend to the high-temperature region. The slowing down of the intensity rise suggests the existence of peak rate temperatures. The transition point can further be defined by taking the derivative for all curves. The peak region of derivatives is enlarged in Fig. 3. The peak shifting feature resembles characteristics of a thermally activated reaction revealed by thermal differential scanning calorimetry (DSC) analysis.[10,11] If we take the RHEED intensity as a thermal reaction variable just as the energy of DTA/DSC, the Kissinger equation can be expressed as

$$\ln\left(\frac{a}{T_{\mathrm{p}}^2}\right) = -\frac{E}{RT_{\mathrm{p}}} + b, \tag{1}$$

where a represents the heating rate, T_{p} represents the peak temperature, R is the gas constant, E is the activation energy and b is a constant. The Kissinger plot of our RHEED data is shown in Fig. 4, where the effective activation energy is 4 eV. From the peak temperature shift in the derivative RHEED intensity, an activated reaction can thus be defined by the Kissinger plot.

The activation energy obtained from Kissinger plot of increasing temperature is close to that of the Arrhenius plot of the constant temperature annealing in ref. 5, in which the kink site unit-cell-removing activation energies of Ti–O and Sr–O were estimated as 3.8 ± 0.3 eV and 3.3 ± 0.2 eV, respectively.

To summarize, we conducted a series of room-temperature depositions of strontium titanate films, and annealed these films at different heating rates. The peak temperature shift of the RHEED derivatives at different heating rates suggests that the steep rise in RHEED intensity is due to an activated mechanism from the poorly crystallized STO films. By adopting the Kissinger method of thermal analysis, we obtained an effective activation energy of 4 eV, which is close to the reported kink-site-removing energy limit.

Acknowledgements

This work was partly supported by the National Science Council of Taiwan under grants NSC91-2112-M009-049.

1) J. H. Neave, B. A. Joyce, P. J. Dobson and N. Norton: Appl. Phys. A **31** (1983) 1.
2) D. M. Holmes, J. L. Sudijono, C. F. McConville, T. S. Jones and B. A. Joyce: Surf. Sci. **370** (1997) L173.
3) J. Y. Lee, J. Y. Juang, K. H. Wu, T. M. Uen and Y. S. Guo: Surf. Sci. **488** (2001) 277.
4) J. H. Neave, P. J. Dobson, B. A. Joyce and J. Zhang: Appl. Phys. Lett. **47** (1985) 100.
5) M. Lippmaa, N. Nakagawa and M. Kawasaki: Appl. Phys. Lett. **76** (2000) 2439.
6) J. Y. Lee, T. C. Wang, S. F. Chen, J. Y. Juang, J. Y. Lin, K. H. Wu, T. M. Uen and Y. S. Gou: Chin. J. Phys. **39** (2001) L299.
7) T. C. Wang, J. Y. Juang, K. H. Wu, T. M. Uen and Y. S. Gou: Jpn. J. Appl. Phys. **43** (2004) 771.
8) J. Y. Lee: PhD Dissertation, National Chiao-Tung University, Taiwan, 2001.
9) H. Y. Lee, W. D. Chang, C. H. Hsu, K. S. Liang, J. Y. Lee, J. Y. Juang, K. H. Wu, T. M. Uen and Y. S. Gou: Thin Solid Films **418** (2002) 163.
10) H. E. Kissinger: Anal. Chem. **29** (1957) 1702.
11) L. C. Chen and F. Spaepen: J. Appl. Phys. **69** (1991) 679.